A numerical framework for simulation of swirled adhesive application

A numerical framework for simulation of swirled adhesive application

Simon Ingelsten[1,2], Roland Kádár[2], Andreas Mark[1] and Fredrik Edelvik[1]
[1] Fraunhofer-Chalmers Research Centre for Industrial Mathematics, 412 88 Gothenburg, Sweden
[2] Division of Engineering Materials, Department of Industrial and Materials Science, Chalmers University of Technology, Gothenburg SE-412 96, Sweden

ABSTRACT

A numerical framework for simulation of swirled adhesive application along arbitrary robot motions and substrate geometries is presented. The momentum and continuity equations are solved on a Cartesian octree grid using a finite volume discretization. A viscoelastic constitutive model is used to describe the complex rheology of the adhesive and is solved using a previously presented Lagrangian-Eulerian method. The flow from the nozzle to the target surface is modelled using experimental data, and a projected injection model is used to add adhesive material in the simulation close to the surface. The two-phase flow of adhesive and air is then simulated. Numerical results are compared with experimental data and good agreement is found.

INTRODUCTION

Hybrid joining techniques have gained attention due to an increased demand for products with new combinations of materials. In many applications adhesive bonding plays an important role. A relatively new technique is swirled adhesive application, in which the material flows from a small nozzle rotating at high speed. The result is a spiral-like bead pattern of the adhesive bead. The main advantage compared to the common cylinder bead is that the application can be performed at larger distances, at higher robot speeds and is less sensitive to geometry variations.

The swirl application is performed with a small circular nozzle, with diameter on the scale of a millimeter or less. In Figure 1, a schematic picture of the swirl nozzle is shown.

In order to predict and optimize the process, and to fully utilize its capabilities, efficient simulation tools are required. In the current work, a method to simulate the complex process is therefore presented. The framework is based on IPS IBOFlow®, an incompressible finite volume flow solver developed at the Fraunhofer-Chalmers Centre in Gothenborg, Sweden. The solver includes a Lagrangian-Eulerian method for viscoelastic flow[13] and has previously been used to simulate two-phase flows with shear thinning fluids for seam sealing[8,10,12] and adhesive extrusion[11]. Other applications include conjugate heat transfer[7] and fluid-structure interaction[9].

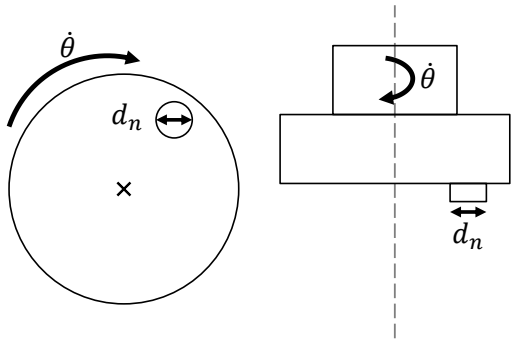

Figure 1. Schematic of swirl nozzle as seen from below (left) and from the side (right).

The adhesives considered are typically complex viscoelastic materials. Several constitutive models exist, suitable for different types of viscoelastic fluids. Examples span from the simpler models of linear viscoelasticity, e.g. the Upper-Convected Maxwell (UCM) model and the Oldroyd-B model[2], to more physically correct models such as the Finitely Extensi-

ble Nonlinear Elasticity (FENE) models[3], the Giesekus model[2] and the Phan Thien Tanner (PTT) model[1].

From a modelling point of view, four important properties for the flows considered in this work can be distinguished:

1. Two-phase flow of the adhesive and the surrounding air.
2. Arbitrary substrate geometry.
3. Viscoelastic material rheology.
4. Moving application along a prescribed path.

The involved equations and the numerical modelling corresponding to each of the respective properties are described further on in this paper.

The rest of the paper is structured as follows. First the governing equations are stated, followed by a description of the numerical method. Results from numerical simulations are then shown and compared to experimental measurements. Finally, conclusions are drawn and some outlines are discussed.

GOVERNING EQUATIONS

The flow is described by the momentum and continuity equations

$$\rho \frac{\partial \mathbf{u}}{\partial t} + \rho \mathbf{u} \cdot \nabla \mathbf{u} = -\nabla p + \nabla \cdot \tau + \mathbf{f}, \tag{1}$$

$$\nabla \cdot \mathbf{u} = 0, \tag{2}$$

where $\mathbf{u}$ is velocity, ρ density, p pressure, τ deviatoric stress, $\mathbf{f}$ body force and t is time. The deviatoric stress can be written as

$$\tau = 2\mu \mathbf{S} + \tau_v, \tag{3}$$

where μ is the Newtonian contribution to viscosity, $\mathbf{S}$ the rate of strain tensor

$$\mathbf{S} = \frac{1}{2}\left(\nabla \mathbf{u} + (\nabla \mathbf{u})^T\right), \tag{4}$$

and τ_v the viscoelastic stress. The constitutive equation from the Phan-Thien-Tanner (PTT) model in its linear form is used to describe the evolution of τ_v as

$$\lambda \overset{\triangledown}{\tau}_v + \left(1 + \frac{\varepsilon \lambda}{\eta} \mathrm{Trace}(\tau_v)\right) \tau_v = 2\eta \mathbf{S}, \tag{5}$$

where λ is relaxation time, η polymeric viscosity, ε a non-dimensional parameter and $\overset{\triangledown}{\tau}$ is the upper-convected derivative

$$\overset{\triangledown}{\tau} = \frac{d\tau}{dt} - \nabla \mathbf{u}^T \cdot \tau - \tau \cdot \nabla \mathbf{u}. \tag{6}$$

It is remarked that d/dt denotes the material, or Lagrangian, time derivative.

Free-surface flow is modelled with the Volume of Fluid (VOF) method. The respective phases are then tracked through the local volume fraction $\alpha \in [0,1]$ by the following transport equation,

$$\frac{\partial \alpha}{\partial t} + \mathbf{u} \cdot \nabla \alpha = 0. \tag{7}$$

If only air is present $\alpha = 1$ and if only adhesive is present $\alpha = 0$. A location where $0 < \alpha < 1$ lies on the interface between the phases. Local fluid properties, e.g. density or viscosity, are calculated as

$$\phi = \alpha \phi_{\mathrm{air}} + (1-\alpha)\phi_{\mathrm{adh}}, \tag{8}$$

where ϕ_{air} is the property of the air and ϕ_{adh} that of the adhesive.

NUMERICAL METHOD

The momentum and continuity equations are solved on an Eulerian grid using a collocated finite volume-discretization and the pressure-velocity coupling is solved using the SIMPLEC method. Interior objects are treated with the mirroring immersed boundary method[5,6]. The velocity field is then implicitly mirrored across the immersed boundary surface such that the defined boundary condition is satisfied for the converged solution. A boundary-conforming

computational mesh is therefore not required and a Cartesian octree grid is used. The grid is automatically generated and updated dynamically simulation progresses. Specifically the grid is refined near the VOF-interface and automatically updated as the interface moves. The resulting numerical framework is suitable for flows with arbitrary geometries, moving objects and free surface flow.

The advective term in (7) for the volume fraction α discretized using the CICSAM scheme[4]. The scheme is specifically designed to maintain a sharp interface between the two phases. This is particularly important since (7) has no natural diffusive term.

The viscoelastic stresses are calculated using a Lagrangian-Eulerian method in which the constitutive equations are solved in Lagrangian nodes that are distributed in the viscoelastic domain and convected by the velocity field. The solution of (5) is thus reduced to solving an ODE system in each Lagrangian node. The updated viscoelastic stresses are interpolated from the unstructured node set to the cell centers of the Eulerian grid using radial basis functions. The stress divergence can then be integrated using Gauss divergence theorem and added as a pseudo-body force to the discretized momentum equation. To ensure a well-distributed node set, nodes are added and deleted where needed in each time step. The method is described in detail in Ingelsten et al.[13].

The final key component of the simulation framework is the injection of adhesive material in the simulation. In the real process, the adhesive flows continuously from the nozzle. In the simulation framework this is modelled by adding material in each time step by modifying the local volume fraction α and setting an appropriate inlet condition. The geometry and state of the added adhesive is determined from an injection model. The injection is performed along the predefined robot path. The position of the injection therefore varies during the simulation and the velocity of the nozzle is added to that of the injected material.

Two main injection model types may be distinguished, namely direct and projected injection models. In the former the material is injected directly at the current position of nozzle and according to the nozzle geometry. Depending on the type of application, this method may require high spatial and temporal resolution to capture the flow from the nozzle to the target surface. This is particularly the case if the application distance is large or if the inlet velocity is large. If this is the case, a projected injection model may be a possible remedy to reduce the computational time. In the projected approach, the main part of the flow between the nozzle and the target surface is instead modelled using data from experiments or detailed numerical simulations. The model is then used to predict the state of the material close to impact on the target surface, where it is injected and the free surface flow is simulated.

The projected injection model for the swirled application is based on a

torus geometry where material is injected in torus segments calculated from the angular velocity of the nozzle $\dot{\theta}$, a given torus radius r_t and the nozzle diameter d_n. The center-point of the torus is calculated by projecting the nozzle position in the application direction using a ray-trace technique.

In the ith time step with length Δt_i, the angle swept, assuming constant angular velocity, is $\Delta\theta_i = \dot{\theta}\Delta t_i$. Material is thus injected in the torus segment defined by angles $\theta \in [\theta_{i-1}, \theta_{i-1} + \Delta\theta_i]$, where θ_{i-1} is the angle from the previous time step. In other words $\theta_i = \theta_{i-1} + \Delta\theta_i$. A schematic view of the injection geometry is shown in Figure 2.

The value of the torus radius r_t is unknown and need to be calculated. In this work, a model is proposed in which r_t depends on the angular velocity, the adhesive flow rate and the application distance, such that

$$r_t = r_t(\dot{\theta}, \dot{V}, L_{\text{app}}), \tag{9}$$

where $\dot{V}$ is the volume flow rate of adhesive from the nozzle and L_{app} is the distance from the nozzle to the substrate surface. An estimate for $r_t(\dot{\theta}, \dot{V}, L_{\text{app}})$ is obtained from experimental data by applying adhesive with different

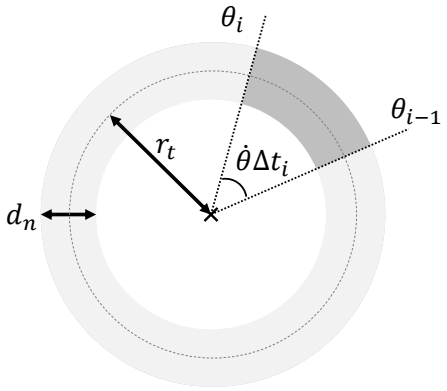

Figure 2. Schematic of torus segment used in the swirl injection model.

process conditions and measuring the radius r_t. The values are stored in a database and during simulation the value of r_t is linearly interpolated for the current process conditions.

The injection procedure may be summarized in the following steps:

1. Find the impact/torus center using ray-tracing
2. Calculate the torus radius $r_t(\dot{\theta}, \dot{V}, L_{\text{app}})$
3. Calculate the torus segment
4. Refine the computational grid around the torus segment
5. Identify injection cells and add material

In the following section, simulations with the proposed method are presented and compared to experimental results.

RESULTS

A set of point clouds of scanned experimental straight beads on a flat plate are available. The experiments and the scanning are performed by RISE IVF in Mölndal, Sweden. The data is then used to measure the bead width for different process conditions and create the database for the torus radius r_t. In Table 1 the process conditions for the experiments are shown. All beads are applied at distance 30 mm from the surface and with application speed 300 mm/s. The nozzle diameter is 0.6 mm. In Figure 3 the scanned experimental beads are shown. It is clear that a combination of high rotation speed and low flow rate as in setup C results in a narrow bead and a dense pattern. The opposite, i.e. low rotation speed and high flow rate (setup B), results in a wider bead with a sparse pattern.

Setup	R (rpm)	$\dot{V}$ (ml/s)
A	10000	1.14
B	10000	1.7
C	20000	1.4
D	20000	1.7

Table 1. Process parameters for the available experiments adhesive beads.

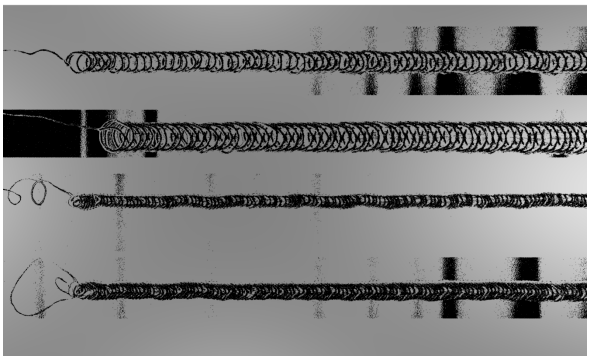

Figure 3. Experimental swirl beads for setup A-D ordered from the top.

In Figure 4 a snapshot from the simulation of setup B as defined in Table 1 is shown. The injection cells are visualized by solid cubes and the adhesive by the contour surface $\alpha = 0.5$, i.e. the interface between the adhesive and the air. The torus segment geometry of the injection zone is clearly visible. In Figure 5 more snapshots from the same simulation can be seen, showing the simulation progress.

In Figure 6 the simulated and experimental beads corresponding to setup A and B in Table 1 are shown. A good overall agreement is found between simulated and experimental beads. This is of course expected to some extent, since the model for the bead width is based on the experiment. It is however remarked that there is also good agreement to the frequency of the spiral-like bead pattern and the overall shape of the bead. In Figure 7 the corresponding results for setup C and D are shown. For these higher rotational speeds the spiral-

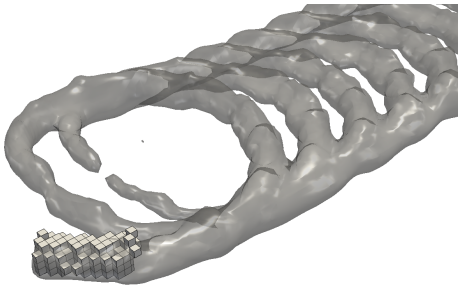

Figure 4. Bead geometry as the contour surface $\alpha = 0.5$. Injection cells shown as solid cubes. Simulated with setup B.

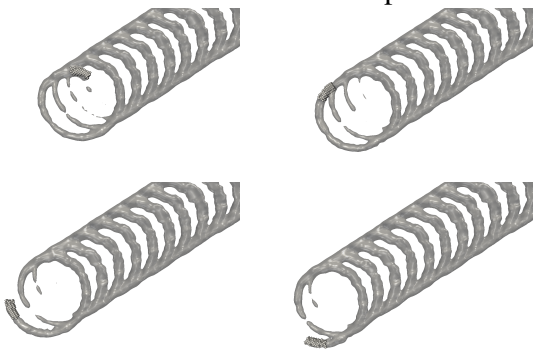

Figure 5. Progression of applied adhesive bead in simulation. Simulated with setup B.

like pattern is denser and the bead widths are smaller than for setups A and B. In the simulation this results in a bead where the pattern is still clearly visible, but without gaps between the individual threads. In the experimental beads, some gap is seen. For all beads, however, the size and frequency in the bead pattern show good agreement with the experiments.

CONCLUSIONS

A numerical framework to simulate swirled application of a viscoelastic adhesive has been presented and demonstrated. The adhesive flow from the nozzle to the impact on the target surface is modelled based on the impact pattern from experimental beads. Adhesive material is then injected close to the surface with an injection model based on a torus-segment geometry. The results show good agreement with experimental data. The obtained results are an important step towards simulating the full mechanical joining process, including part assembly and hemming with adhesives.

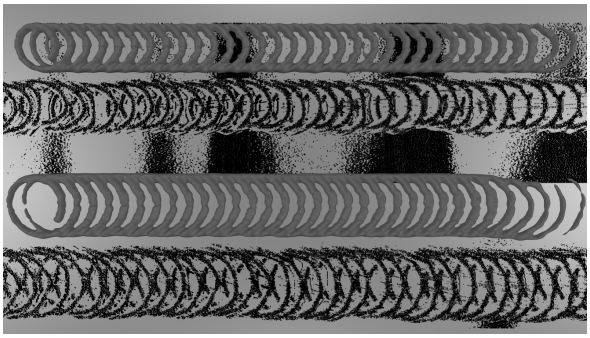

Figure 6. Comparison between simulated and experimental swirl beads for setup A (top) and B (bottom).

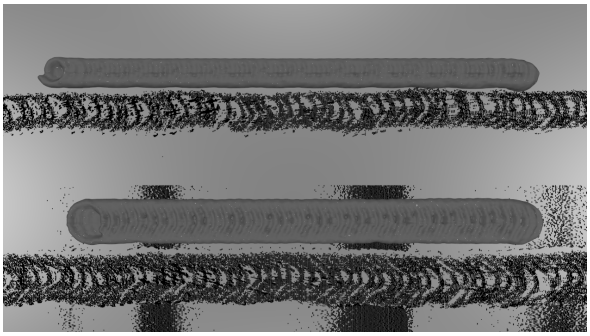

Figure 7. Comparison between simulated and experimental swirl beads for setup C (top) and D (bottom).

ACKNOWLEDGEMENTS

This work has been supported in part by the Swedish Governmental Agency for Innovation Systems, VINNOVA, through the FFI Sustainable Production Technology program, and in part by the Production Area of Advance at Chalmers University of Technology. The support is gratefully acknowledged. Scanned experimental data and rheology measurements were obtained from RISE IVF.

REFERENCES

1. Thien, N. P. and Tanner, R. I. (1977), "A new constitutive equation derived from network theory", *Journal of Non-Newtonian Fluid Mechanics*, **2**, 353–365.

2. Larson, R. G. (1988), "Constitutive Equations for Polymer Melts and Solutions", Butterworth Publishers.

3. Herrchen, M. and Öttinger, H. C. (1997), "A detailed comparison of various FENE dumbbell models", *Journal of Non-Newtonian Fluid Mechanics*, **68**, 17 - 42.

4. Ubbink, O. and Issa, R. (1999), "A Method for Capturing Sharp Fluid Interfaces on Arbitrary Meshes", *Journal of Computational Physics*, **153**, 26 - 50.

5. Mark, A. and Wachem, B. G. M. (2008), "Derivation and validation of a novel implicit second-order accurate immersed boundary method", *J. of Comput. Physics*, **227**, 6660 - 6680.

6. Mark, A., Rundqvist, R. and Edelvik, F. (2011), "Comparison Between Different Immersed Boundary Conditions for Simulation of Complex Fluid Flows", *Fluid dynamics & materials processing*, **7**, 241-258.

7. Mark, A., Svenning, E. and Edelvik, F. (2013), "An immersed boundary method for simulation of flow with heat transfer", *International Journal of Heat and Mass Transfer*, **56**, 424 - 435.

8. Mark, A., Bohlin, R., Segerdahl, D., Edelvik, F. and Carlson, J. S. (2014), "Optimisation of robotised sealing stations in paint shops by process simulation and automatic path planning", *International Journal of Manufacturing Research*, **9**, 4-26.

9. Svenning, E., Mark, A. and Edelvik, F. (2014), "Simulation of a highly elastic structure interacting with a two-phase flow", *Journal of Mathematics in Industry*, **4**, 7.

10. Mark, A., Ingelsten, S. and Edelvik, F. (2016), "Lay Down Simulation of Viscoelastic Fluids Using the Hybrid Immersed-Boundary Method", *ICMF-2016 – 9th International Conference on Multiphase Flow, May 22nd – 27th 2016, Firenze, Italy*,.

11. Svensson, M., Mark, A., Edelvik, F., Kressin, J., Bohlin, R., Segerdahl, D., Carlson, J. S. et al. (2016), "Process Simulation and Automatic Path Planning of Adhesive Joining", *Procedia CIRP*, **44**, 298 - 303.

12. Edelvik, F., Mark, A., Karlsson, N., Johnson, T. and Carlson, J. (2017), "Math-Based Algorithms and Software for Virtual Product Realization Implemented in Automotive Paint Shops", 231-251.

13. Ingelsten, S., Mark, A. and Edelvik, F. (2019), "A Lagrangian-Eulerian framework for simulation of transient viscoelastic fluid flow", *Journal of Non-Newtonian Fluid Mechanics*, **266**, 20 - 32.